




ARTICLE

Population pharmacokinetic dosimetry model using imaging data to assess variability in pharmacokinetics of ^{177}Lu -PSMA-617 in prostate cancer patients

Hinke Siebinga^{1,2}  | Bastiaan M. Privé³ | Steffie M. B. Peters³ | James Nagarajah³ | Thomas P. C. Dorlo^{1,4}  | Alwin D. R. Huitema^{1,5,6} | Berlinda J. de Wit-van der Veen²  | Jeroen J. M. A. Hendriks^{1,2}

¹Department of Pharmacy & Pharmacology, The Netherlands Cancer Institute, Amsterdam, The Netherlands

²Department of Nuclear Medicine, The Netherlands Cancer Institute, Amsterdam, The Netherlands

³Department of Radiology and Nuclear Medicine, Radboud University Medical Center, Nijmegen, The Netherlands

⁴Department of Pharmacy, Uppsala University, Uppsala, Sweden

⁵Department of Clinical Pharmacy, University Medical Center Utrecht, Utrecht University, Utrecht, The Netherlands

⁶Department of Pharmacology, Princess Máxima Center for Pediatric Oncology, Utrecht, The Netherlands

Correspondence

Jeroen J. M. A. Hendriks, Department of Pharmacy & Pharmacology, The Netherlands Cancer Institute, Plesmanlaan 121, 1066 CX Amsterdam, The Netherlands.

Email: j.hendriks@nki.nl

Abstract

Studies to evaluate and optimize [^{177}Lu]Lu-PSMA treatment focus primarily on individual patient data. A population pharmacokinetic (PK) dosimetry model was developed to explore the potential of using imaging data as input for population PK models and to characterize variability in organ and tumor uptake of [^{177}Lu]Lu-PSMA-617 in patients with low volume metastatic prostate cancer. Simulations were performed to identify the effect of dose adjustments on absorbed doses in salivary glands and tumors. A six-compartment population PK model was developed, consisting of blood, salivary gland, kidneys, liver, tumor, and a lumped compartment representing other tissue (compartment 1–6, respectively), based on data from 10 patients who received [^{177}Lu]Lu-PSMA-617 (2 cycles, ~3 and ~6 GBq). Data consisted of radioactivity levels (decay corrected) in blood and tissues (9 blood samples and 5 single photon emission computed tomography/computed tomography scans). Observations in all compartments were adequately captured by individual model predictions. Uptake into salivary glands was saturable with an estimated maximum binding capacity (B_{max}) of 40.4 MBq (relative standard error 12.3%) with interindividual variability (IIV) of 59.3% (percent coefficient of variation [CV%]). IIV on other PK parameters was relatively minor. Tumor volume was included as a structural effect on the tumor uptake rate constant (k_{15}), where a two-fold increase in tumor volume resulted in a 1.63-fold increase in k_{15} . In addition, interoccasion variability on k_{15} improved the model fit (43.5% [CV%]). Simulations showed a reduced absorbed dose per unit administered activity for salivary glands after increasing radioactivity dosing from 3 to 6 GBq (0.685 Gy/GBq vs. 0.421 Gy/GBq, respectively). All in all, population PK modeling could help to improve future radioligand therapy research.

This is an open access article under the terms of the [Creative Commons Attribution-NonCommercial-NoDerivs](https://creativecommons.org/licenses/by-nc-nd/4.0/) License, which permits use and distribution in any medium, provided the original work is properly cited, the use is non-commercial and no modifications or adaptations are made.

© 2023 The Authors. *CPT: Pharmacometrics & Systems Pharmacology* published by Wiley Periodicals LLC on behalf of American Society for Clinical Pharmacology and Therapeutics.

Study Highlights

WHAT IS THE CURRENT KNOWLEDGE ON THE TOPIC?

Multiple single photon emission computed tomography (SPECT)/computed tomography (CT) scans are obtained after administration of [^{177}Lu]Lu-PSMA, but little research has been conducted into population trends of [^{177}Lu]Lu-PSMA uptake.

WHAT QUESTION DID THIS STUDY ADDRESS?

This study aimed to explore the potential of using data derived from SPECT/CT scans as input for population pharmacokinetic (PK) models. A population PK dosimetry model was developed to characterize variability in organ and tumor uptake of [^{177}Lu]Lu-PSMA-617 in patients with low volume metastatic prostate cancer and to simulate effects of dose adjustments on absorbed doses in salivary glands and tumors.

WHAT DOES THIS STUDY ADD TO OUR KNOWLEDGE?

A six-compartment model characterized variability in [^{177}Lu]Lu-PSMA distribution. Salivary gland uptake was saturable and simulations showed a reduced absorbed dose per unit administered activity for salivary glands after increased radioactivity dosing. Besides, dose individualization could potentially be based on tumor volume, because increased tumor volumes resulted in increasing uptake in tumors.

HOW MIGHT THIS CHANGE DRUG DISCOVERY, DEVELOPMENT, AND/OR THERAPEUTICS?

Enriching current research on dosimetry with population PK models could help to improve and personalize radioligand therapy.

INTRODUCTION

Radioligand therapy has shown favorable effects on advanced stage prostate cancer (PCa) in the recently published phase III VISION trial.¹ For this treatment, prostate-specific membrane antigen (PSMA) peptide is radiolabeled with Lutetium-177 (^{177}Lu) and after intravenous administration, it targets the PSMA-overexpressing PCa cells with high specificity.² Although this promising approach has resulted in complete disappearance of PCa lesions in some patients, in the general population, responses are heterogeneous as are the observed radiation-induced organ toxicities. Research regarding [^{177}Lu]Lu-PSMA treatment focusses predominantly on methods to improve the therapeutic index and optimize treatment by, for example, applying alternative (individualized) dosing regimens or introducing new PSMA-targeting ligands.³

To quantify absorbed radiation doses in organs and tumor lesions (often referred to as “dosimetry”), multiple single photon emission computed tomography (SPECT)/computed tomography (CT) scans are obtained on various timepoints after administration of [^{177}Lu]Lu-PSMA.⁴ In the clinical setting, dosimetry is used to estimate patient-specific radiation doses in treatment-limiting organs or tumor lesions to guide therapy. However, little research has

been conducted into population trends of [^{177}Lu]Lu-PSMA uptake. Jackson et al. introduced a population approach, where information of multiple individuals was gathered to eventually estimate individual [^{177}Lu]Lu-PSMA-617 absorbed doses based on a single measurement.⁵ This approach of using population data to limit the number of sampling timepoints is quite similar to a Bayesian therapeutic drug monitoring approach. Still, their approach only focused on specific treatment-limiting organs instead of describing a full pharmacokinetic (PK) profile and how uptake in specific regions might be related to each other.

Population PK modeling, using nonlinear mixed-effects models (NLMEMs), might be a valuable tool to improve the dosimetry of [^{177}Lu]Lu-PSMA therapy based on limited post-administration scans and to identify and add knowledge on covariates influencing population dosimetry. Such models can describe total PK behavior and are not limited to tissue retention as observed on post-administration scans. Moreover, the models are able to describe variability on PK parameters and specific uptake into different predefined compartments. Applying this approach to develop a population dosimetry model will lead to a more comprehensive understanding of population exposure and variability in whole-body [^{177}Lu]Lu-PSMA distribution than traditional dosimetry models based on integration of the radioactivity-time curve (or time-activity curve) based on blood sample

or scan data. In addition, these models are a proven tool in pharmacological research to acquire extra information, for example, regarding covariates affecting uptake into compartments or variability in uptake between different treatment cycles.^{6,7} Such knowledge can be used to optimize individual absorbed dose estimations, and eventually even personalize dosing regimens, for example, by using Bayesian therapeutic drug monitoring methods to guide dose adjustment by estimating effects on tumor and organ uptake.⁸ Nuclear imaging data are not regularly used as input for these PK modeling approaches. However, because nuclear imaging data are subject to a high level of noise, using NLMEMs would be an appropriate approach for disentangling residual unexplained variability (noise) from interindividual variability (IIV) and interoccasion variability (IOV) on the parameter level.

Therefore, the primary aim of this project was to explore the potential of using [¹⁷⁷Lu]Lu-PSMA-617 uptake data derived from multiple SPECT/CT scans as input for population PK models. In addition, we aimed to develop a population PK dosimetry model to get a better understanding of PK parameters and to explain variability in organ and tumor uptake of [¹⁷⁷Lu]Lu-PSMA-617 in patients with low volume metastatic PCa. Last, simulations were performed to identify the effect of differences in administered radioactivity on absorbed doses in salivary glands (dose-limiting organ) and tumors.

METHODS

Patients and data

Data from 10 patients with low volume early stage metastatic PCa were available from a prospective clinical study in the Radboud University Medical Center (NCT03828838).⁹ All patients showed PSMA positive lesion(s) on diagnostic [⁶⁸Ga]Ga-PSMA positron emission tomography/CT and received two cycles of [¹⁷⁷Lu]Lu-PSMA-617 with injected activities of ~3 GBq and ~6 GBq with an interval of 8 weeks. After each administration, nine blood samples (5, 30, 60, 120, and 180 min and 24, 48, 72, and 168 h post-injection) and five SPECT/CT scans (1, 24, 48, 72, and 168 h post-injection) were acquired to quantify accumulation profiles. All records regarding radioactivity were corrected for radioactive decay over time by recalculating the measured activity to the corresponding activity at the time of injection. Quantification of SPECT scans was performed by placing volumes-of-interest based on CT contours of organs in salivary glands, liver, kidneys, and tumor lesions, whereas for determining blood activity, multiple regions-of-interest were drawn in the aorta. A detailed description of the image acquisition and dosimetry method was previously published.¹⁰

Model development

Blood compartment

The initial structural model was developed using concentration-time data from the central compartment alone. Both blood sample and blood activity derived from SPECT/CT scan were used as observations for this central compartment. Blood data derived from SPECT scans are subject to a high noise level, whereas blood samples represent more accurate concentration measurements. Therefore, to apply blood activity data from SPECT scans as input for modeling purposes, a linear correction to blood sample data was estimated (following Equation 1). Using Equation 1, all predictions based on SPECT data were corrected to predictions based on blood samples.

$$C_{pred,ij} = C_{pred\ SPECT,ij} * \beta + \alpha \quad (1)$$

where C_{pred} represents the corrected predicted concentration for individual i and observation j , $C_{pred\ SPECT}$ represents the predicted concentration for SPECT data and α and β represent linear correction estimates, with α being the intercept and β the degree of change in corrected concentration prediction for every one unit of change in the predicted concentration based on SPECT data.

In addition, an estimated structural measurement effect (γ) was added to predicted blood concentrations (following Equation 2). This effect explained an assumed difference between measured and actual blood concentration, where actual concentrations were assumed lower because of calibration uncertainty for blood samples caused by extreme calibration ranges. Residual unexplained variability (RUV) was described by two separate combined proportional and additive residual error models (see Equation 2), both for blood sample and SPECT data separately for this blood compartment.

$$C_{obs,ij} = (C_{pred,ij} + \gamma) * (1 + \epsilon_{p,ij}) + \epsilon_{add,ij} \quad (2)$$

C_{obs} represents the observed concentration for individual i and observation j , C_{pred} represents the predicted concentration (corrected in case of SPECT blood data), γ represents the structural measurement effect and ϵ_p and ϵ_{add} represent the proportional and additive error, respectively, both distributed with mean zero and variance ω^2 .

Dosimetry model

Subsequently, this model for blood data was expanded to a six-compartment model, consisting of a blood (1), salivary glands (2), kidneys (3), liver (4), tumor (5) compartment, and a rest compartment representing other tissue (6).

Salivary glands, kidneys, and tumor compartments were lumped, meaning that these compartments represented all salivary glands, both kidneys and all tumor lesions, respectively. Elimination was described by an excretion rate constant (k_{10}) and drug transport between the central compartment and all other compartments was described by rate constant (k) parameters. Volume of distribution was only estimated for the central compartment, and, consequently, observations and predictions for all other compartments were in amounts (MBq) rather than concentrations (MBq/L). An overview of the population PK dosimetry model structure is depicted in Figure 1.

Models for saturable binding equilibria were tested for all organ and tumor compartments (following Equation 3), because PSMA ligand uptake into organs and tumors is mainly driven by binding to the PSMA receptor and subsequent internalization of the receptor-ligand complex.^{11–13}

$$\frac{dA}{dt} = k_{in} * A_{blood} * \left(1 - \frac{A_{target}}{B_{MAX}}\right) - k_{out} * A_{target} \quad (3)$$

where k_{in} and k_{out} represent the rate constants, A_{blood} and A_{target} represent the compound amounts in the blood and target compartment, respectively, and B_{MAX} is the maximum binding capacity in the target compartment (i.e., PSMA receptor expression).

The IIV was evaluated for the excretion rate (k_{10}), B_{MAX} in case of saturable binding, and all rate constant parameters to compartments 2, 3, 4 and 5, following

Equation 4. The IOV, with each cycle defined as a separate occasion, was tested to take into account cycle-to-cycle variability. IOV was implemented similarly to IIV (see Equation 4). Last, RUV was described by a separate proportional residual error model for each compartment (see Equation 5).

$$P_i = P_{pop} * e^{\eta_i} \quad (4)$$

$$C_{obs,ij} = C_{pred,ij} * (1 + \varepsilon_{p,ij}) \quad (5)$$

where P represents the PK parameter estimate for individual i , P_{pop} represents the population PK parameter estimate, and η represents the IIV or IOV effect for individual i with mean zero and variance ω^2 . C_{obs} represents the observed concentration for individual i and observation j , C_{pred} represents the predicted concentration and ε_p represent the proportional error, distributed with mean zero and variance ω^2 .

Structural effects

No extensive covariate testing was performed, because the patient population was rather small as well as expected ranges in patient characteristics. Only structural effects that were expected to describe part of the mechanism-based population PK model were tested to improve the model fit. These structural effects identify relationships between patient-specific factors and structural model

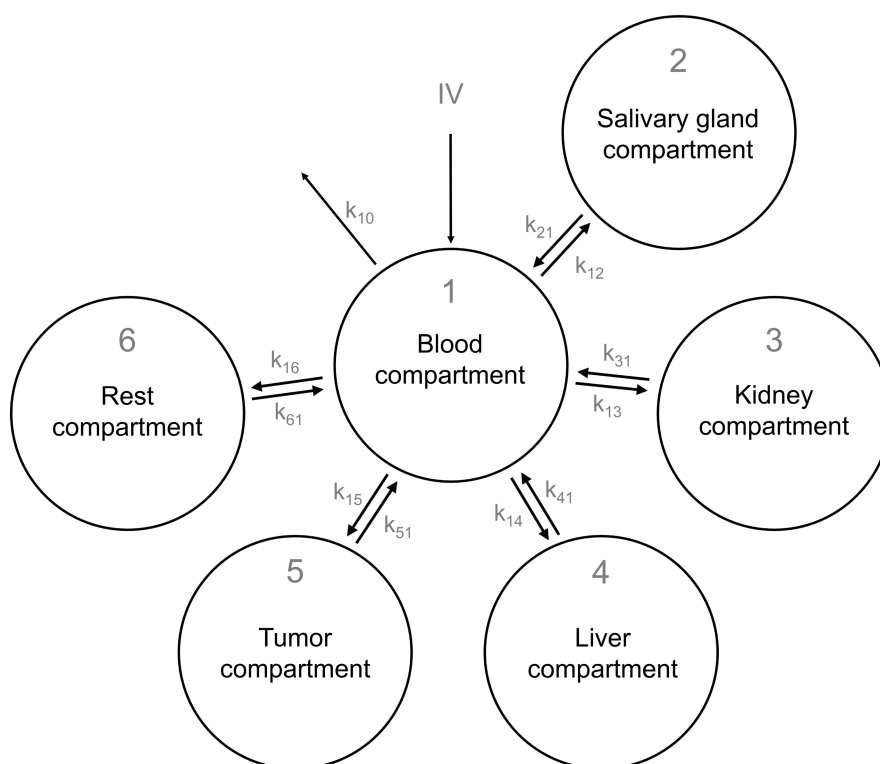


FIGURE 1 Overview of the six-compartment model structure for [¹⁷⁷Lu]Lu-PSMA-617

parameters. PSMA ligand uptake in tumors is related to tumor aggressiveness, which is reflected by (among others) tumor volume and the prostate-specific antigen (PSA) level.^{14–18} Therefore, total tumor volume (determined before the start of each treatment cycle) and (baseline) PSA were both tested as a structural effect on tumor uptake (k_{15}). These continuous structural effects were evaluated using linear and power functions. Cell death in salivary glands due to radiation is a possible cause of decreased salivary gland uptake in later cycles,¹⁹ thus, the second treatment cycle was tested as a (dichotomous) structural effect on salivary gland uptake (k_{12}) or B_{MAX} (if identified). [¹⁷⁷Lu]Lu-PSMA-617 is renally excreted, thus, creatinine clearance (calculated using the Cockcroft-Gault equation) was added on k_{10} a priori, using a linear function with the assumption of complete renal elimination.^{20,21}

Model selection and evaluation

Model selection was guided by evaluation of goodness-of-fit (GOF) plots, precision of estimated parameters, and change in objective function values (OFVs). In case of hierarchical modeling, an OFV drop of greater than or equal to 3.84 points (corresponding to a p value < 0.05, following a chi-square distribution with 1 degree of freedom) was considered a significant improvement of the model fit. Eventually, models were evaluated with GOF plots, visual predictive checks (VPCs), and parameter uncertainty, which was assessed using the sampling importance resampling (SIR) method.²²

Absorbed dose simulations

Using the final model parameters, simulations were performed for salivary glands and tumor for both dosing regimens (until time after administration of 168 h). Radioactivity-time curves were simulated for a typical patient with median patient characteristics after administration of 3 and 6 GBq [¹⁷⁷Lu]Lu-PSMA-617. For each simulation, 1000 patients were simulated and estimated IIV and RUV were taken into account in these simulations. Based on these simulations, absorbed doses were calculated for salivary glands and tumors for both administered doses using the Medical Internal Radiation Dose calculation (see Equation 6).²³ Organ weights that were used for absorbed dose calculations were based on the International Commission on Radiological Protection (ICRP) Publication 89 adult male human model and corresponding S-values, similar to calculations by Peters et al.^{10,24}

$$D = \tilde{A} * S \quad (6)$$

where D represents the absorbed dose in tissue (mGy), \tilde{A} represents the time-integrated activity in tissue (MBq*h), and S is the common S-value for physical effects (mGy/MBq*h).

Software

Modeling was performed using NONMEM (version 7.5; ICON development Solutions, Ellicott City, MD) using the first-order conditional estimation method with interaction (FOCE-I) and ADVAN13. R (version 4.1.3) was used for data processing, model evaluation by visualization of GOF plots and VPCs, and simulations based on the final model.

RESULTS

Patients

Data from 10 patients with low volume metastatic PCa that received two cycles of [¹⁷⁷Lu]Lu-PSMA-617 were used for model development, with a total of 180 blood samples and 491 SPECT/CT scan observations available. Kidney data from SPECT scans acquired at ~1 h were excluded from analysis, because those observations were expected to mainly represent urine activity instead of intracellular kidney uptake. Total liver radioactivity contains a major contribution of ¹⁷⁷Lu in the blood within the liver because of a high vascularization, so radioactivity within liver blood volume (calculated from the reference hepatic blood volume) was subtracted from total measured liver activity.²⁵ Median (range) total tumor volume was 2.14 ml (0.27–76.6 ml) before study inclusion and decreased to 0.92 ml (0.27–78.0 ml) before start of the second treatment cycle. Patient characteristics are shown in Table 1, additional patient characteristics and information regarding previous treatment is published previously.⁹ Radioactivity-time curves of [¹⁷⁷Lu]Lu-PSMA-617 in the population are shown for all compartments in Figures S1–S5.

Population pharmacokinetic dosimetry model

Blood compartment

The initial model was developed to accurately describe blood sample data, using both blood sample and imaging-derived blood data. Blood activity derived from SPECT scans seemed suitable for model development, using an estimated linear correction with $\alpha = 6.27$ MBq/L and $\beta = 0.828$. The structural measurement effect γ was

estimated 0.273 MBq/L. These parameter values were fixed in further model development. Results from individual predictions of blood concentrations based on SPECT blood data input, using the estimated correction, compared to blood sample data are shown in Figure 2.

TABLE 1 Patient characteristics and demographics (baseline values as measured at study inclusion, unless stratified per cycle)

Characteristic	Median (range)
Age (years)	67 (61–77)
Weight (kg)	84.0 (59.4–97.0)
Height (cm)	178 (174–182)
Creatinine clearance (ml/min)	87.9 (50.2–110)
Hemoglobin (g/dl)	9.1 (8.0–10.5)
ALT (U/L)	21.5 (13–32)
AST (U/L)	22 (12–28)
PSA (ng/ml)	1.75 (0.43–20)
Gleason score	8.5 (7–9)
Total tumor volume (ml)	
Cycle 1	2.14 (0.27–76.6)
Cycle 2	0.92 (0.27–78.0)
Injected radioactivity (MBq)	
Cycle 1	3064 (3025–3155)
Cycle 2	6039 (4972–6073)

Abbreviations: ALT, alanine transaminase; AST, aspartate transaminase; PSA, prostate-specific antigen.

Dosimetry model

A six-compartment model with first-order kinetics adequately described the available activity observations in most compartments, except for an underprediction of measured liver activity at early timepoints. Final model parameter estimates for k_{in} differed between the organ and tumor compartments and were 0.0238 h^{-1} for k_{12} (salivary glands), 0.00867 h^{-1} for k_{13} (kidneys), 0.0238 h^{-1} for k_{14} (liver), and 0.000248 h^{-1} for k_{15} (tumor). In addition, k_{out} was lower for tumor (0.00902 h^{-1}) compared with organs (0.0307 h^{-1} , 0.0141 h^{-1} , and 0.0283 h^{-1} for salivary glands, kidneys, and liver, respectively). The volume of the central compartment was estimated 10.3 L. Saturable uptake into the salivary glands improved model fits for this compartment with an estimated B_{MAX} of 40.4 MBq. For other compartments, there was no successful estimation of B_{MAX} (liver) or model fits did not improve (kidney and tumor). IIV was added on k_{10} , k_{13} , k_{41} , k_{15} , and B_{MAX} . For k_{10} , k_{13} (kidneys), and k_{41} (liver), IIV was very small (17.2%, 16.1%, and 9.5% coefficient of variation [CV%], respectively), whereas IIV on B_{MAX} in salivary glands and the tumor uptake rate constant were higher (59.3% and 58.8% [CV%] for B_{MAX} and k_{15} , respectively).

Structural effects

Tumor volume was incorporated on k_{15} (tumor), using a power covariate function, with an estimated value of 0.705

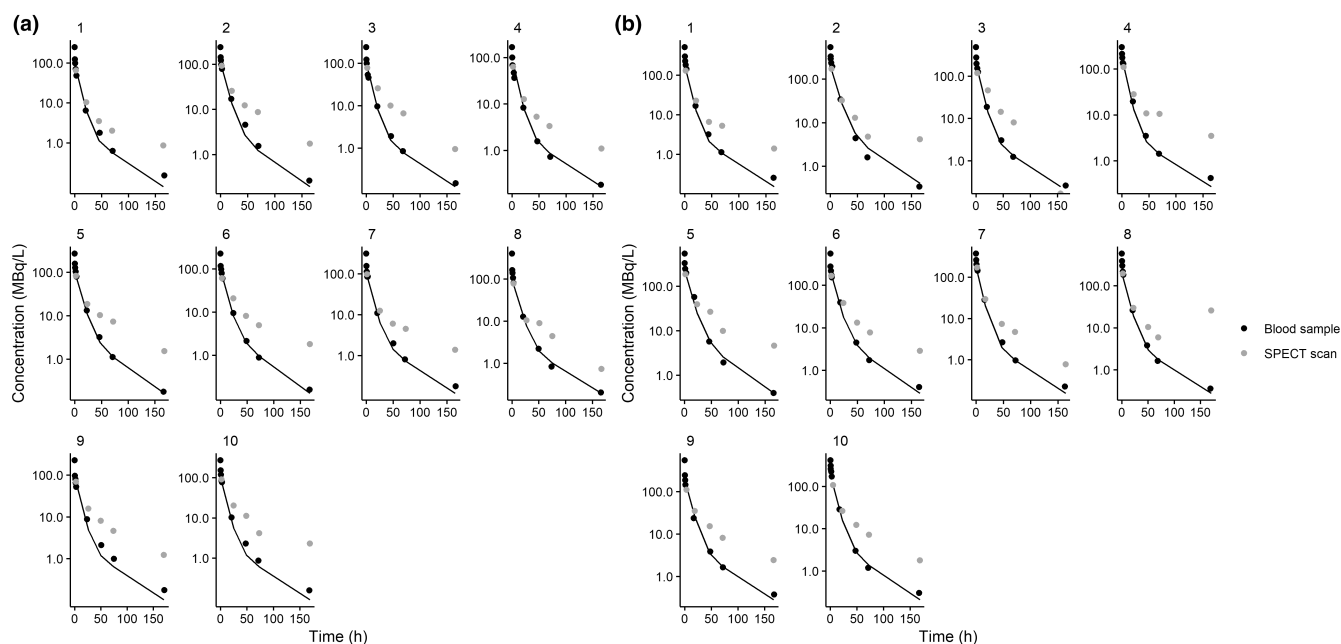


FIGURE 2 Individual predictions (IPRED) based on blood data derived from single photon emission computed tomography (SPECT) scans (solid line) versus blood observations from both blood samples (black dots) and SPECT scans (gray dots) for treatment cycles 1 (a) and 2 (b)

(relative standard error [RSE] 12.3%). This structural effect resulted in significant decrease in OFV (dOFV -23.9) and GOF plots showed an improved model fit. With inclusion of this identified effect, a two-fold increase in tumor volume compared to the median results in a 1.63-fold increase in k_{15} . Addition of PSA on k_{15} to the base model also resulted in a significant decrease in OFV, although this effect was less pronounced (dOFV -8.38) and plots showed worse predictions of the observed data compared to adding tumor volume. Based on these results along with a known correlation between PSA and tumor volume, only tumor volume and not PSA was added as structural effect on k_{15} in the final model. Furthermore, the second treatment cycle was tested on the B_{MAX} (receptor expression in salivary glands), but model fits did not improve. Last, IOV added on k_{15} (tumor) significantly improved model fit (dOFV -63.4) and was estimated 43.5% (CV%).

Model evaluation

SIR results showed RSEs less than 20% for all structural PK parameters, IIVs, and IOVs. All final model parameter estimates, 95% confidence intervals, and parameter uncertainties are shown in Table 2. GOF plots showed accurate prediction of observed data within all compartments. In addition, conditional weighted residuals (CWRES) seemed normally distributed over prediction and time intervals, except for the liver compartment (see Figure 3). Individual prediction plots for all compartments are shown in Figures S2–S5. The VPC showed that model simulations including intervals were capable to describe mean observations and the 90% confidence interval of observed data (see Figure 4). However, GOF plots and the VPC showed an underprediction in the liver for all observations at early timepoints.

Absorbed dose simulations

Radioactivity-time simulations for salivary glands and tumor based on the final model are shown in Figure 5. These simulations clearly showed the effect of saturable uptake in salivary glands. Absorbed dose in salivary glands based on this population simulation was 2.06 Gy (range 1.85–2.26 Gy) and 2.53 Gy (range 2.26–2.80 Gy) after administration of 3 and 6 GBq, respectively. In other words, cumulative absorbed dose per unit administered activity was higher for 3 GBq dosing compared to 6 GBq (0.685 Gy/GBq vs. 0.421 Gy/GBq, respectively). For tumors, absorbed dose was calculated using the median tumor volume (1.73 ml) and a corresponding S-value of 0.0114 mGy/MBq*s. Tumor absorbed dose based on

TABLE 2 Final model parameter estimates and parameter uncertainties for the six-compartment model, representing a blood (1), salivary gland (2), kidney (3), liver (4), tumor (5), and rest compartment (6)

	Estimate (RSE%)	95% CI
Structural parameters		
k_{10} (h ⁻¹)	0.288 (7.6)	0.248–0.335
k_{12} (h ⁻¹)	0.0238 (12.4)	0.0184–0.0302
k_{21} (h ⁻¹)	0.0307 (5.8)	0.0276–0.0346
k_{13} (h ⁻¹)	0.00867 (8.6)	0.00725–0.0102
k_{31} (h ⁻¹)	0.0141 (4.7)	0.0128–0.0154
k_{14} (h ⁻¹)	0.0238 (7.9)	0.0204–0.0276
k_{41} (h ⁻¹)	0.0283 (4.6)	0.0260–0.0310
k_{15} (h ⁻¹)	0.000248 (14.0)	0.000181–0.000317
k_{51} (h ⁻¹)	0.00902 (11.4)	0.00753–0.0103
k_{16} (h ⁻¹)	1.05 (15.3)	0.837–1.27
k_{61} (h ⁻¹)	0.744 (7.9)	0.622–0.871
V1 (L)	10.3 (4.5)	9.40–11.3
B_{MAX} compartment 2 (MBq)	40.4 (12.3)	31.4–50.8
IIV (CV%)		
k_{10}	17.2 (13.7)	15.0–19.4
k_{13}	16.1 (16.8)	14.0–18.2
k_{41}	9.5 (16.8)	7.3–10.6
k_{15}	58.8 (17.3)	31.6–76.7
B_{MAX} compartment 2	59.3 (15.8)	49.4–67.8
Structural effects		
Tumor volume on k_{15}	0.705 (12.3)	0.532–0.865
IOV (CV%)		
k_{15}	43.5 (15.1)	35.2–48.7
RUV (proportional, CV%)		
Compartment 1 (blood samples)	19.3 (11.5)	17.2–21.6
Compartment 1 (SPECT data)	56.0 (12.4)	49.4–62.8
Compartment 2	24.6 (11.7)	21.6–27.1
Compartment 3	30.4 (11.2)	26.7–33.4
Compartment 4	85.0 (12.9)	73.8–95.6
Compartment 5	45.8 (12.9)	39.6–50.9
RUV (additive)		
Compartment 1 ^a (MBq/L)	0.25	

Note: 95% CI and RSE values were obtained from the SIR.

Abbreviations: B_{MAX} , maximum binding capacity; CL, clearance; CI, confidence interval; CV%, coefficient of variation; IIV, interindividual variability; IOV, interoccasion variability; RSE, relative standard error; RUV, residual unexplained variability; SIR, sampling importance resampling; SPECT, single photon emission computed tomography; V1, central volume of distribution.

^aBoth for blood sample data as for data derived from SPECT scans.

simulations increased from 8.10 Gy (range 6.73–9.46 Gy) to 16.2 Gy (range 13.5–19.0 Gy) after a dose increase from 3 to 6 GBq [¹⁷⁷Lu]Lu-PSMA-617.

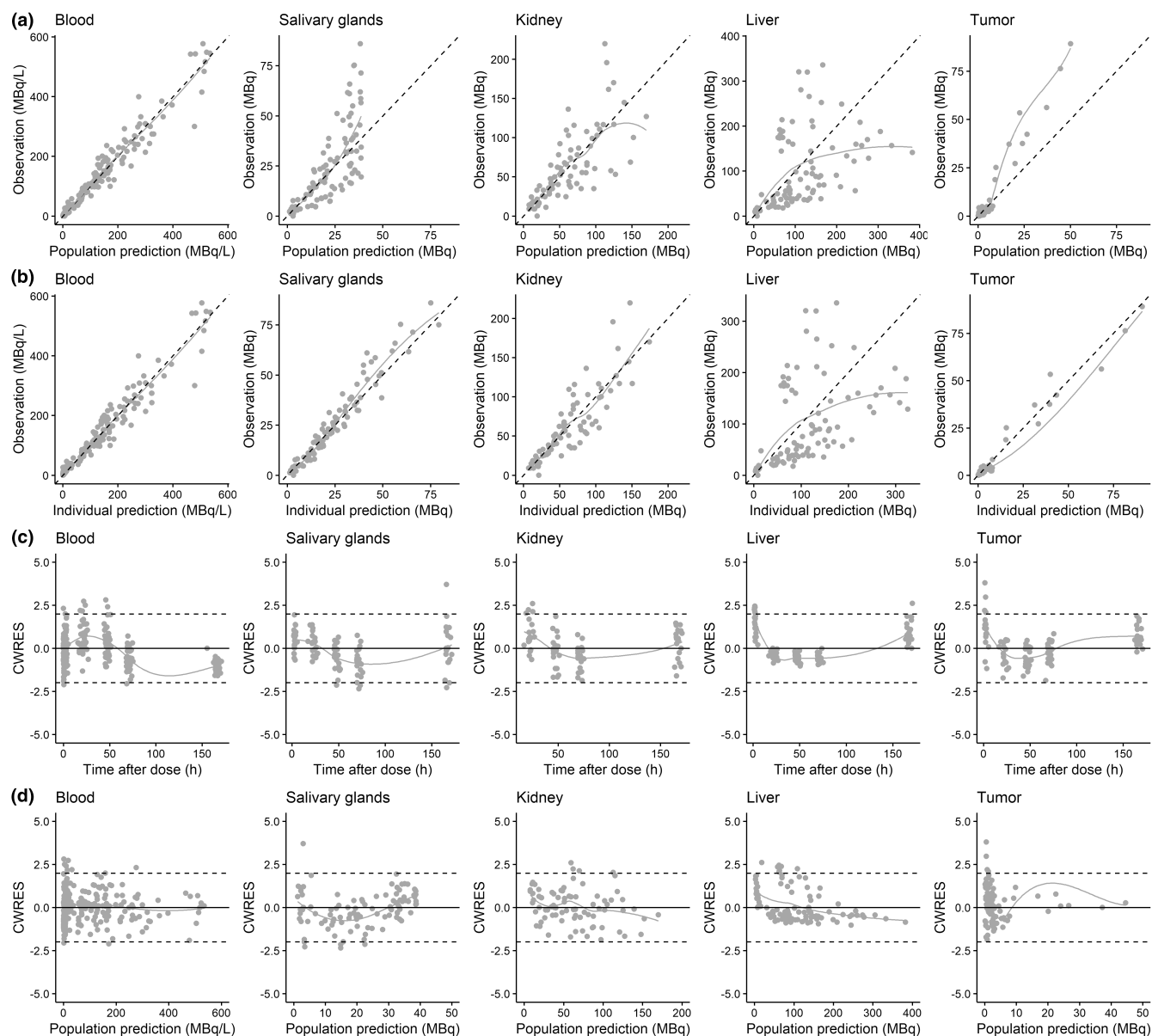


FIGURE 3 Goodness-of-fit plots of the final model for [^{177}Lu]Lu-PSMA-617, including population predictions (PRED) versus observations (a), individual predictions (IPRED) versus observations (b), conditional weighted residuals (CWRES) versus time after dose (c) and CWRES versus PRED (d), for all compartments separately

DISCUSSION

A six-compartment PK dosimetry model, using a NLMEM approach, was developed for [^{177}Lu]Lu-PSMA-617 in patients with low volume metastatic PCa. Population PK models are a well-accepted approach for model-informed drug development and are regularly used to identify variability sources and covariates that can affect drug exposure. Our multicompartment structure resembles a (population) physiologically-based pharmacokinetic (PBPK) model, but an empirical approach was used and estimated PK parameters were not derived from predefined physiological processes and drug-specific parameters. Therefore, there was no need for exact information

(with related assumptions) on many input parameters, and this simpler, “PBPK-like,” approach was preferable to identify variability on overall uptake into compartments in this population. Using this approach, model results still showed an accurate description of individual observed data. In addition, in future research, population PK models could improve research regarding comparison of different PSMA ligands, enhancement of dose predictions for individual patients (using identified covariates), and prediction of expected therapy effects (e.g., using PSA levels).

Nuclear imaging data proved suitable for model development and the final model adequately predicted radioactivity uptake in all compartments (blood, salivary glands, kidneys, liver, and tumors), although liver observations at

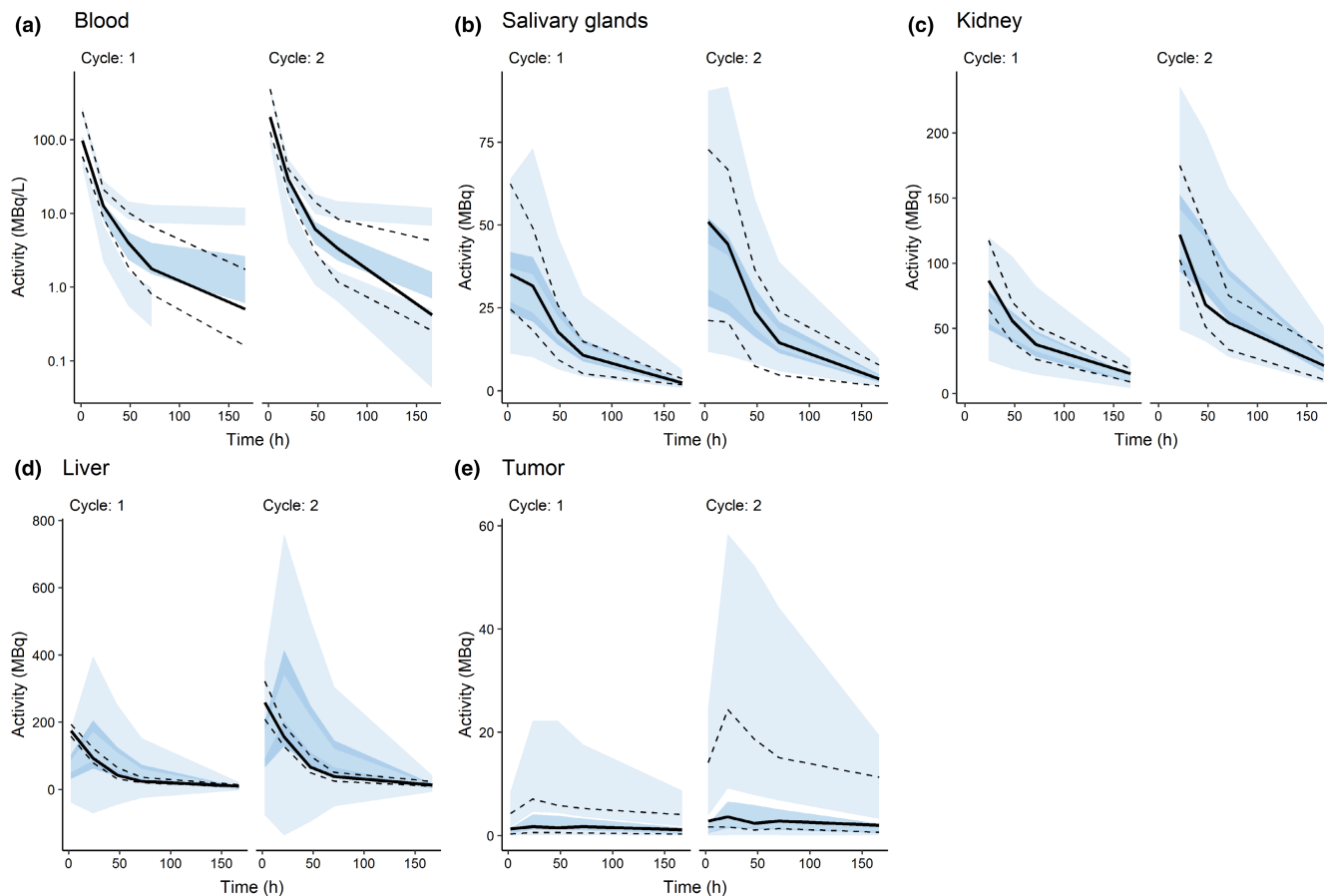


FIGURE 4 Visual predictive check (VPC) of the final population pharmacokinetic (PK) model for [^{177}Lu]Lu-PSMA-617 stratified per treatment cycle, based on 1000 simulations. Solid lines and dashed lines represent median observed values and 5th and 95th percentiles of observed values, whereas dark and light blue areas represent 80% confidence intervals of the simulated median and 5th and 95th percentiles of simulated values

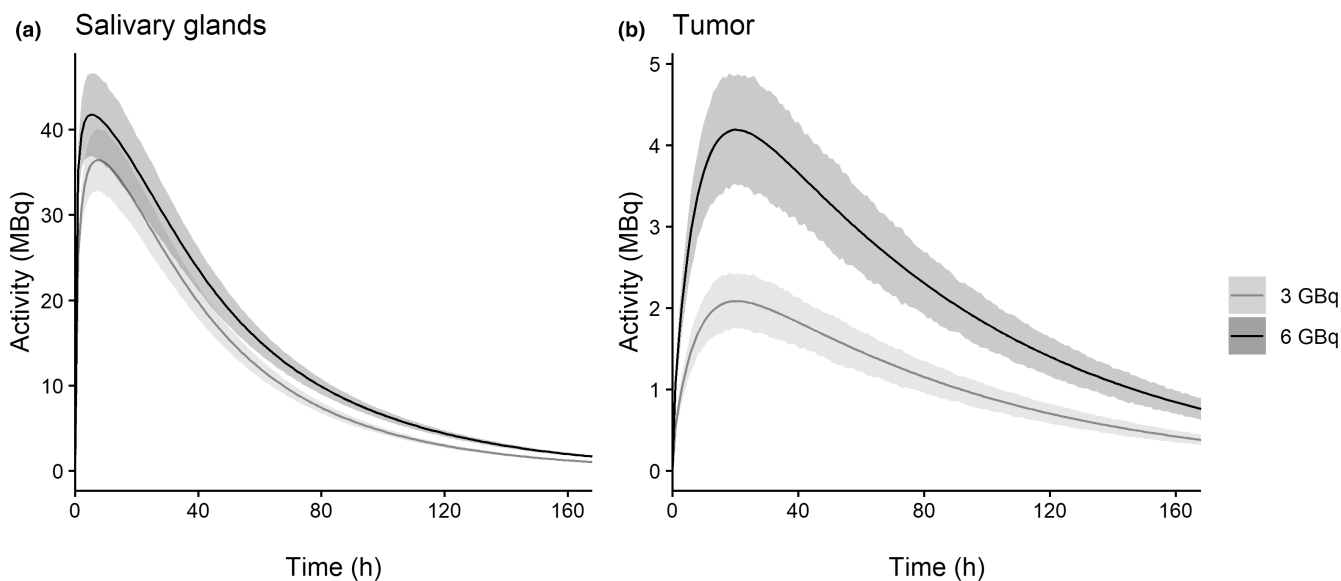


FIGURE 5 Simulated population radioactivity-time curves for [^{177}Lu]Lu-PSMA-617 in salivary glands and tumor after administration of 3 GBq (gray) and 6 GBq (black), where solid lines represent geometric mean and shaded areas represent 95% confidence intervals of the simulated mean ($n = 1000$ per dose level)

early timepoints were underpredicted. Findings based on this developed model provided new insights regarding variability and its sources within this PCa patient population and showed relatively small IIV on most PK parameters and an IOV of 43.5% (CV%) on the tumor uptake rate constant (k_{15}). Besides estimating PK parameters and population variability, simulations showed that absorbed dose per unit administered activity in salivary glands (dose limiting organ) lowered with increasing administered radioactivity, whereas absorbed dose in tumor lesions increased. Still, it has to be noted that all patients used for model development received 3 GBq in their first and 6 GBq in the second treatment cycle. This difference in treatment cycles between low and high radioactivity dose may have impacted organ and tumor accumulation, because radiation effects could lead to a persistent reduction of uptake in later cycles. However, “treatment cycle” was not identified as having an effect on salivary gland uptake, thus the timing of dosing regimens was not likely to impact our simulations. Hence, the estimated saturable salivary gland uptake hints toward a safe increase of the radioactivity dose for this population, with potential improved efficacy due to higher absorbed tumor doses.¹⁰ Future individualized [^{177}Lu]Lu-PSMA-617 dosing could potentially be based on tumor volume, which had a structural effect on k_{15} , where an increased tumor volume resulted in an increased tumor uptake rate (a two-fold increase in tumor volume resulted in a 1.63-fold increase in k_{15}). By any means, a first step would be extrapolating this model to a patient population with larger total tumor burden representing the population commonly treated in clinical practice. While extrapolating to such a population, the effect of tumor load on normal organ uptake is a factor to consider.^{26–28}

As this is the first population PK model published for [^{177}Lu]Lu-PSMA, results cannot directly be compared. However, [^{177}Lu]Lu-DOTATATE has a similar mechanism of action regarding receptor binding and internalization, and the excretion rate constant of 0.288 h^{-1} for [^{177}Lu]Lu-PSMA-617 was comparable to 0.204 h^{-1} reported for [^{177}Lu]Lu-DOTATATE.²⁹ Estimated PK parameters were clearly different for tumors compared with other organs, which was partly caused by absolute radioactivity amounts being relatively small in tumors compared with organs due to volume differences between compartments. In addition, accumulation profiles appeared different (see Figures S1–S5) and the achieved maximum concentration and slower elimination were described by smaller k_{in} and k_{out} rate estimates for tumor compared with organs. For all PSMA-expressing compartments, the rate parameter back to the central compartment was higher compared to the uptake rate into the specific compartment. For tumors, this effect was most pronounced, which was caused by the very low total amounts of activity in the tumor compartment compared to blood.

To the best of our knowledge, variability on PK parameters was not assessed previously for [^{177}Lu]Lu-PSMA-617. Using this NLMEM approach, part of the variability on the uptake rate for tumor (k_{15}) was described by an inter-cycle difference (IOV 43.5% [CV%]). This identified cycle-to-cycle variability was expected to play a part in radioligand therapy based on clinical observations and could be caused by patient conditions, such as hydration status, as well as treatment effects or tumor progression. Still, this high inter-cycle variability on k_{15} could hamper therapy individualization based on predefined tumor absorbed doses. Future research with additional data can improve disentangling sources describing this variability. In addition to IOV, the uptake rate for tumor (k_{15}) showed a higher IIV compared to the uptake rate for kidneys (k_{13}). A possible explanation for this difference could be that tumor exhibits the highest PSMA ligand uptake compared with other tissues and thus the uptake rate constant is more likely to vary.^{11,26} In addition, IIV in receptor expression might explain high variability in uptake for tumors, which was also identified for salivary glands with an IIV of 59.3% (CV%) on the maximum binding capacity (i.e., receptor expression). This B_{MAX} for salivary glands might be overestimated, because PSMA-specific uptake was assumed, whereas PSMA ligand uptake in salivary glands is not necessarily exclusively PSMA-specific.³⁰ This assumption was primarily based on reasons of model simplicity, but also because the debate regarding this nonspecific uptake is still ongoing.

The proportional RUV was higher for blood data derived from scan data (56.0% [CV%]) compared to blood sample data (19.3% [CV%]), which reflects the higher noise content for scan data. Furthermore, for this blood compartment, CWRES plots (Figure 3c) implied a misspecification for later timepoints. This underprediction was partly caused by the estimated structural measurement effect (γ) for blood data, which forced predictions to be lower than observations with an estimated value of 0.273 MBq/L (see Equation 2), of which the effect was more pronounced for lower observations. Second, GOF plots included both SPECT and sample data for the blood compartment. This also resulted in an underprediction, because SPECT blood data were purposely corrected to (lower) blood sample concentrations to account for the high noise level, especially for low radioactivity concentrations at later timepoints. Considering this all and based on visual inspection of SPECT prediction results (see Figure 2), blood activity data derived from nuclear imaging data seemed suitable for model input after correction to blood samples. Of course, the estimated linear correction requires further evaluation, to assure correct extrapolation of this correction to, for example, other PSMA ligands or patient populations.

VPC results (Figure 4) and individual liver predictions (Figure S4) showed a discrepancy between liver

observations and predictions at timepoints <24 h post-injection. Whereas liver activity data and these model results implied nonlinear elimination from the liver compartment, unfortunately, there is no clear explanation for this potential nonlinearity. After all, data observations include measured activity in the whole liver and, for example, distribution to another compartment would have been included within the observed data. The nonlinearity is presumably also not caused by saturable uptake, because the addition of this effect did not result in a successful estimation. An explanation for this could be that, although PSMA ligand uptake is observed, PSMA receptor expression in healthy tissue is fairly limited.^{11,26,31–33}

Despite that the addition of tumor volume as a structural effect on k_{15} significantly improved the model fit, a misspecification for high observations in the tumor remained. However, all observations that were clearly underpredicted (see Figure 3a) belonged to one patient with a higher total tumor volume (76.6 ml in the first cycle) compared with all other patients. Therefore, absolute uptake (in MBq) into tumor lesions was also higher and, apparently, our model was not yet capable of adequately describing uptake in this large tumor. Relevance of this tumor volume effect needs to be evaluated and presumably optimized with extra data, including patients with larger tumor burden, which is also more representative for the clinical population currently receiving [¹⁷⁷Lu]Lu-PSMA-617 treatment.

To conclude, this population PK dosimetry model adequately described [¹⁷⁷Lu]Lu-PSMA-617 uptake in salivary glands, kidneys, liver, and tumors lesions in patients with low volume metastatic PCa. Our approach proved imaging data suitable for model development, even for blood activity with use of a correction factor. IIV on most PK parameters was rather small and IOV on the tumor uptake rate constant was estimated 43.5% (CV%). This tumor uptake rate constant increased with increasing tumor volume, which could be relevant for future dose individualization. Furthermore, salivary gland uptake was saturable and simulations showed that increasing radioactivity dosing from 3 to 6 GBq resulted in a reduced cumulative absorbed dose per unit administered activity for salivary glands, whereas for tumors, this increased with higher administered radioactivity doses. Population PK modeling using NLMEMs could help to improve future radioligand therapy research, particularly as post-administration scans will become more commonly available with the increased interest in dosimetry.

AUTHOR CONTRIBUTIONS

H.S. wrote the manuscript. J.J.M.A.H., B.J.dW-vdV., A.D.R.H., and H.S. designed the research. H.S., A.D.R.H., and T.P.C.D. performed the research. B.M.P., S.M.B.P., and J.N. analyzed the data.

FUNDING INFORMATION

Partial financial support was received from the Radboud Oncology Foundation and the Dutch Prostate Cancer Foundation during the conduct of the initial prospective study. No funds, grants, or other support were received for conducting this study.

CONFLICT OF INTEREST

J.N. has received research support from Novartis, a consulting fee from CURIUM and a speaker honorarium from Bayer outside the submitted work. All other authors declared no competing interests for this work.

ORCID

Hinke Siebinga  <https://orcid.org/0000-0001-7767-0393>
 Thomas P. C. Dorlo  <https://orcid.org/0000-0003-3076-8435>
 Berlanda J. de Wit-van der Veen  <https://orcid.org/0000-0002-7860-2904>

REFERENCES

1. Sartor O, de Bono J, Chi KN, et al. Lutetium-177-PSMA-617 for metastatic castration-resistant prostate cancer. *N Engl J Med*. 2021;385(12):1091–1103. doi:10.1056/NEJMoa2107322
2. Silver DA, Pellicer I, Fair WR, Heston WD, Cordon-Cardo C. Prostate-specific membrane antigen expression in normal and malignant human tissues. *Clin Cancer Res*. 1997;3(1):81–85.
3. Jackson P, Hofman M, McIntosh L, Buteau JP, Ravi KA. Radiation dosimetry in (177)Lu-PSMA-617 therapy. *Semin Nucl Med*. 2021;52(2):243–254. doi:10.1053/j.semnuclmed.2021.11.003
4. Sjögreen Gleisner K, Chouin N, Gabina PM, et al. EANM dosimetry committee recommendations for dosimetry of 177Lu-labelled somatostatin-receptor- and PSMA-targeting ligands. *Eur J Nucl Med Mol Imaging*. 2022;49(6):1778–1809. doi:10.1007/s00259-022-05727-7
5. Jackson PA, Hofman MS, Hicks RJ, Scalzo M, Violet J. Radiation dosimetry in (177)Lu-PSMA-617 therapy using a single posttreatment SPECT/CT scan: a novel methodology to generate time- and tissue-specific dose factors. *J Nucl Med*. 2020;61(7):1030–1036. doi:10.2967/jnumed.119.233411
6. Ette EI, Williams PJ, Lane JR. Population pharmacokinetics III: design, analysis, and application of population pharmacokinetic studies. *Ann Pharmacother*. 2004;38(12):2136–2144. doi:10.1345/aph.1E260
7. Mould DR, Upton RN. Basic concepts in population modeling, simulation, and model-based drug development-part 2: introduction to pharmacokinetic modeling methods. *CPT Pharmacometrics Syst Pharmacol*. 2013;2:e38. doi:10.1038/psp.2013.14
8. Donagher J, Martin JH, Barras MA. Individualised medicine: why we need Bayesian dosing. *Intern Med J*. 2017;47(5):593–600. doi:10.1111/imj.13412
9. Prive BM, Peters SMB, Muselaers CHJ, et al. Lutetium-177-PSMA-617 in low-volume hormone-sensitive metastatic prostate cancer: a prospective pilot study. *Clin Cancer Res*. 2021;27(13):3595–3601. doi:10.1158/1078-0432.CCR-20-4298
10. Peters SMB, Prive BM, de Bakker M, et al. Intra-therapeutic dosimetry of [(177)Lu]Lu-PSMA-617 in low-volume hormone-sensitive metastatic prostate cancer patients and

- correlation with treatment outcome. *Eur J Nucl Med Mol Imaging*. 2022;49(2):460-469. doi:10.1007/s00259-021-05471-4
11. Afshar-Oromieh A, Hetzheim H, Kratochwil C, et al. The Theranostic PSMA ligand PSMA-617 in the diagnosis of prostate cancer by PET/CT: biodistribution in humans, radiation dosimetry, and first evaluation of tumor lesions. *J Nucl Med*. 2015;56(11):1697-1705. doi:10.2967/jnumed.115.161299
 12. Benešová M, Schäfer M, Bauder-Wüst U, et al. Preclinical evaluation of a tailor-made DOTA-conjugated PSMA inhibitor with optimized linker moiety for imaging and Endoradiotherapy of prostate cancer. *J Nucl Med*. 2015;56(6):914-920. doi:10.2967/jnumed.114.147413
 13. Afshar-Oromieh A, Babich JW, Kratochwil C, et al. The rise of PSMA ligands for diagnosis and therapy of prostate cancer. *J Nucl Med*. 2016;57(Suppl 3):79s-89s. doi:10.2967/jnumed.115.170720
 14. Rüschhoff JH, Ferraro DA, Muehlematter UJ, et al. What's behind (68)Ga-PSMA-11 uptake in primary prostate cancer PET? Investigation of histopathological parameters and immunohistochemical PSMA expression patterns. *Eur J Nucl Med Mol Imaging*. 2021;48(12):4042-4053. doi:10.1007/s00259-021-05501-1
 15. Lojanapiwat B, Anutrakulchai W, Chongruksut W, Udomphot C. Correlation and diagnostic performance of the prostate-specific antigen level with the diagnosis, aggressiveness, and bone metastasis of prostate cancer in clinical practice. *Prostate Int*. 2014;2(3):133-139. doi:10.12954/pi.14054
 16. Carter HB. Differentiation of lethal and non lethal prostate cancer: PSA and PSA isoforms and kinetics. *Asian J Androl*. 2012;14(3):355-360. doi:10.1038/aja.2011.141
 17. Jochumsen MR, Sörensen J, Tolbod LP, et al. Potential synergy between PSMA uptake and tumour blood flow for prediction of human prostate cancer aggressiveness. *EJNMMI Res*. 2021;11(1):12. doi:10.1186/s13550-021-00757-y
 18. Siebinga H, Olde Heuvel J, Rijkhorst EJ, Hendriks J, de Wit-van der Veen BJ. The impact of peptide amount on tumor uptake to assess PSMA receptor saturation on (68)Ga-PSMA-11 PET/CT in primary prostate cancer patients. *J Nucl Med*. 2023;64(1):63-68. doi:10.2967/jnumed.122.264101
 19. Heynickx N, Herrmann K, Vermeulen K, Baatout S, Aerts A. The salivary glands as a dose limiting organ of PSMA- targeted radionuclide therapy: a review of the lessons learnt so far. *Nucl Med Biol*. 2021;98-99:30-39. doi:10.1016/j.nucmed-bio.2021.04.003
 20. Wester H-J, Schottelius M. PSMA-targeted radiopharmaceuticals for imaging and therapy. *Semin Nucl Med*. 2019;49(4):302-312. doi:10.1053/j.semnuclmed.2019.02.008
 21. Cockcroft DW, Gault MH. Prediction of creatinine clearance from serum creatinine. *Nephron*. 1976;16(1):31-41. doi:10.1159/000180580
 22. Dosne AG, Bergstrand M, Karlsson MO. An automated sampling importance resampling procedure for estimating parameter uncertainty. *J Pharmacokinet Pharmacodyn*. 2017;44(6):509-520. doi:10.1007/s10928-017-9542-0
 23. Bolch WE, Eckerman KF, Sgouros G, Thomas SR. MIRD pamphlet No. 21: a generalized schema for radiopharmaceutical dosimetry--standardization of nomenclature. *J Nucl Med*. 2009;50(3):477-484. doi:10.2967/jnumed.108.056036
 24. Basic anatomical and physiological data for use in radiological protection: reference values. A Report of Age- and Gender-Related Differences in the Anatomical and Physiological Characteristics of Reference Individuals. ICRP Publication 89. Ann ICRP. 2002;32(3-4):5-265.
 25. Eipel C, Abshagen K, Vollmar B. Regulation of hepatic blood flow: the hepatic arterial buffer response revisited. *World J Gastroenterol*. 2010;16(48):6046-6057. doi:10.3748/wjg.v16.i48.6046
 26. Gaertner FC, Halabi K, Ahmadzadehfard H, et al. Uptake of PSMA-ligands in normal tissues is dependent on tumor load in patients with prostate cancer. *Oncotarget*. 2017;8(33):55094-55103. doi:10.18632/oncotarget.19049
 27. Gafita A, Wang H, Robertson A, et al. Tumor sink effect in (68)Ga-PSMA-11 PET: myth or reality? *J Nucl Med*. 2022;63(2):226-232. doi:10.2967/jnumed.121.261906
 28. Begum NJ, Thieme A, Eberhardt N, et al. The effect of Total tumor volume on the biologically effective dose to tumor and kidneys for (177)Lu-labeled PSMA peptides. *J Nucl Med*. 2018;59(6):929-933. doi:10.2967/jnumed.117.203505
 29. Puzskiel A, Bauriaud-Mallet M, Bourgeois R, Dierickx L, Courbon F, Chatelut E. Evaluation of the interaction of amino acid infusion on (177)Lu-Dotatate pharmacokinetics in patients with Gastroenteropancreatic neuroendocrine tumors. *Clin Pharmacokinet*. 2019;58(2):213-222. doi:10.1007/s40262-018-0674-1
 30. Rupp NJ, Umbricht CA, Pizzuto DA, et al. First Clinicopathologic evidence of a non-PSMA-related uptake mechanism for (68)Ga-PSMA-11 in salivary glands. *J Nucl Med*. 2019;60(9):1270-1276. doi:10.2967/jnumed.118.222307
 31. Ristau BT, O'Keefe DS, Bacich DJ. The prostate-specific membrane antigen: lessons and current clinical implications from 20 years of research. *Urol Oncol*. 2014;32(3):272-279. doi:10.1016/j.urolonc.2013.09.003
 32. O'Keefe DS, Bacich DJ, Huang SS, Heston WDW. A perspective on the evolving story of PSMA biology, PSMA-based imaging, and Endoradiotherapeutic strategies. *J Nucl Med*. 2018;59(7):1007-1013. doi:10.2967/jnumed.117.203877
 33. O'Keefe DS, Bacich DJ, Heston WD. Comparative analysis of prostate-specific membrane antigen (PSMA) versus a prostate-specific membrane antigen-like gene. *Prostate*. 2004;58(2):200-210. doi:10.1002/pros.10319

SUPPORTING INFORMATION

Additional supporting information can be found online in the Supporting Information section at the end of this article.

How to cite this article: Siebinga H, Privé BM, Peters SMB, et al. Population pharmacokinetic dosimetry model using imaging data to assess variability in pharmacokinetics of ¹⁷⁷Lu-PSMA-617 in prostate cancer patients. *CPT Pharmacometrics Syst Pharmacol*. 2023;12:1060-1071. doi:10.1002/psp4.12914